Acta Cryst. (1989). A45, 478-485

The Electronic Structure of NaF and CaO Studied by Compton Scattering

BY J. REDINGER

Technical University of Vienna, Institute for Techn. Electrochemistry, Getreidemarkt 9, A-1060 Vienna, Austria

R. PODLOUCKY

University of Vienna, Institute of Physical Chemistry, Währingerstrasse 42, A-1090 Vienna, Austria

S. MANNINEN AND T. PITKÄNEN

University of Helsinki, Department of Physics, SF-00170 Helsinki, Finland

AND O. AIKALA

University of Turku, Department of Physical Sciences, SF-20500 Turku, Finland

(*Received* 27 *June* 1988; *accepted* 27 *February* 1989)

Abstract

Compton profiles of NaF and CaO single crystals were measured along the [100] and [110] directions using 60 keV gamma rays. A theoretical analysis based on Compton profiles and autocorrelation functions was performed by application of the augmented plane wave (APW) and linear combination of atomic orbitals (LCAO) methods. In the case of NaF both theories agree well with each other but their results differ in a characteristic manner from the experiment. For CaO a good agreement of the APW results and experiment especially for the difference quantities is found whereas the LCAO model yields less satisfying results in this case.

1. Introduction

In our previous study on MgO (Aikala, Paakkari & Manninen, 1982; Podloucky & Redinger, 1984) we found a discrepancy between the experimental data and both LCAO and APW theories expressed in terms of the Compton profile and autocorrelation function. Despite the laborious effort, including the use of various kinds of wave functions for the O^{2-} ion, the problem was not solved. In particular, there was a clear disagreement between the experimental and theoretical results taken along the [100] direction which is towards the nearest neighbours in this structure.

In order to understand better this characteristic discrepancy, it was decided to carry out an experimental and theoretical study on NaF and CaO single crystals. The former is known to be well described by an ionic wave function for a F^- ion which has the same electron configuration as O^{2-} but is stable as a free F^- ion in contrast to the highly polarizable O^{2-} ion. Consequently, the oxygen ion in CaO is different from the oxygen ion in MgO (Redinger & Schwarz, 1981). We apply an APW and a LCAO model to interpret and analyse the experimental results.

2. Theory

2.1. *APW model*

We define the electron momentum density of a Bloch state with band index ν and wave vector $\mathbf{k}$ by

$$n(\mathbf{k}\nu, \mathbf{p}) = \delta(\mathbf{k}+\mathbf{g}, \mathbf{p}) \int \Psi(\mathbf{k}\nu, \mathbf{r}) \exp(-i\mathbf{p}\,.\,\mathbf{r})\, \mathrm{d}\mathbf{r} \quad (1)$$

where $\Psi(\mathbf{k}\nu, \mathbf{r})$ is normalized within the unit cell. The δ function is set to be 1 if $\mathbf{k}$ and $\mathbf{p}$ differ only by a reciprocal-lattice vector $\mathbf{g}$ and zero otherwise. We obtain the total momentum density by summing over all occupied states

$$n(\mathbf{p}) = \sum_{\nu} \int_{\Omega_{BZ}} n(\mathbf{k}\nu, \mathbf{p}) f(\mathbf{k}\nu)\, \mathrm{d}\mathbf{k} \quad (2)$$

and integrating over the volume Ω_{BZ} of the first Brillouin zone by defining $f(\mathbf{k}\nu) = 1$ for occupied states and zero otherwise. Within the APW model we split the unit cell into two parts, inside and outside the muffin-tin spheres. Inside the spheres the basis functions are described by

$$\varphi_{\mathbf{g}}(\mathbf{k}\nu, \mathbf{r}) = \sum_{l,m} A_{l,m}(\mathbf{k}\nu, \mathbf{g}) R_l(E_\nu, r)\, Y_{l,m}(\mathbf{r}) \quad (3)$$

and outside by a plane wave,

$$\varphi_{\mathbf{g}}(\mathbf{k}\nu, \mathbf{r}) = \exp[i(\mathbf{k}+\mathbf{g})\,.\,\mathbf{r}]. \quad (4)$$

The APW wave function is then obtained by linear combination of the basis functions

$$\Psi(\mathbf{k}\nu, \mathbf{r}) = \sum_{\mathbf{g}} C(\mathbf{k}\nu, \mathbf{g}) \varphi_{\varphi}(\mathbf{k}\nu, \mathbf{r}) \quad (5)$$

and the coefficients $C(\mathbf{k}\nu, \mathbf{g})$ are calculated from the usual variational procedure.

0108-7673/89/070478-08$03.00

Table 1. *Parameters as used in the APW calculation (a.u.)*

	CaO	NaF	MgO
a (lattice constant)	9·106	8·757	7·965
r_A (anion sphere radius)	2·336	2·400	2·304
r_C (cation sphere radius)	2·217	1·979	1·678

The Compton profiles can then be calculated from the momentum density $n(\mathbf{p})$ in a straightforward manner,

$$J_{\hat{\mathbf{n}}}(p_z) = \int n(\mathbf{p})\delta(\hat{\mathbf{n}} \cdot \mathbf{p} - p_z)\, \mathrm{d}\mathbf{p}. \quad (6)$$

From the Compton profiles one can calculate position-space quantities, so-called $B(z)$ functions [which are autocorrelation functions of one-electron wave functions; for details, see Pattison & Weyrich (1979)] by a one-dimensional Fourier inversion

$$B_{\hat{\mathbf{n}}}(z) = \int J_{\hat{\mathbf{n}}}(p_z) \exp(-ip_z z)\, \mathrm{d}p_z. \quad (7)$$

The band structure of NaF and CaO was calculated using the self-consistent symmetrized APW method at the equilibrium lattice constant a. Exchange and correlation were incorporated within the local-density approximation using the Hedin–Lundqvist parametrization. During the iteration cycles the muffin-tin approximation was employed both for the potential and the charge density. The **k** grid consisted of 29 **k** points distributed uniformly over the irreducible wedge of the Brillouin zone including the main symmetry directions. Using up to 96 plane waves all the eigenvalues converged to better than 10^{-3} rydberg ($2{\cdot}17 \times 10^{-21}$ J). The muffin-tin radii were chosen approximately at the charge-density minimum between the neighbouring cations and anions. This choice of radii reflects the prevailing ionic nature of these compounds. The lattice constants and muffin-tin radii are given in Table 1. The momentum density for NaF and CaO was computed from the symmetrized APW's up to a momentum value of $17{\cdot}6\pi/a$. To correct for the cutoff the APW momentum density was augmented by the corresponding ionic densities up to a momentum of 62 a.u. This procedure ensures the correct normalization of the Compton profiles which is important if total profiles are to be compared. The F 1s, O 1s, Na 1s, Ca 1s, Ca 2s and Ca 2p core states were treated as atomic-like states in the self-consistent muffin-tin potential. The core momentum densities and Compton profiles were also calculated up to a momentum of 62 a.u. The $B(z)$ functions themselves were obtained from the corresponding Compton profiles by a straightforward one-dimensional Fourier transform.

2.2. *LCAO model*

All one-electron properties, *e.g.* Compton profiles, can be calculated starting from the first-order density matrix $\rho(\mathbf{r}, \mathbf{r}')$, which in the LCAO approximation for the crystals composed of closed-shell atoms or ions is given by (Löwdin, 1956)

$$\rho(\mathbf{r}, \mathbf{r}') = \sum_{\mu} \sum_{\nu} \Psi_{\mu}(\mathbf{r})(\tilde{\Delta}^{-1})_{\mu\nu} \Psi^*_{\nu}(\mathbf{r}'). \quad (8)$$

Here $\tilde{\Delta}^{-1}$ is the inverse of the metric (or overlap) matrix $\tilde{\Delta}$ with elements

$$\Delta_{\mu\nu} = \int \Psi^*_{\mu}(\mathbf{r})\Psi_{\nu}(\mathbf{r})\, \mathrm{d}\mathbf{r} \quad (9)$$

and the $\Psi_{\mu}(\mathbf{r})$'s are the (known) local orbitals centred on the atoms or ions of the crystal.

To calculate $\tilde{\Delta}^{-1}$ from the local orbitals with the Fourier-series method, which is considered to be the most stable one (Aikala, 1983), the matrix is first partially diagonalized by a unitary transformation (Fourier series) in the same way as the normal coordinates are obtained in the theory of lattice vibrations. The small blocks so obtained are then inverted and the inverse transformation (integration in the Brillouin zone) is used to get elements of the matrix.

The momentum density $n(\mathbf{p})$ is obtained as the double Fourier transform of the density matrix (8) and the Compton profile in the direction **k** is then a one-dimensional projection of $n(\mathbf{p})$ in the direction **k** (see, for example, Williams, 1977). The detailed computing procedures for Slater-type local orbitals are explained elsewhere (Aikala, 1977, and references therein).

The $B(z)$ functions are then calculated as in § 2.1. Here the basis local orbitals (STO's) for Na^+, F^- and Ca^{2+} ions were chosen to be the free-ion wave functions by Clementi (1965). In the case of MgO (Aikala, Paakkari & Manninen, 1982) altogether nine different sets of wave functions for O^{2-} were tested. It was found that in terms of the LCAO model the best agreement with experiment was obtained for that based on a Watson +1 potential well (Watson, 1958) and for the wave function of Pantelides, Mickish & Kunz (1974) based on a band-structure calculation. In addition to these, the wave functions of Schwarz & Schulz (1978) calculated using the Watson sphere with numerical Slater-type orbital fitting and of Abarenkov & Antonova (1979) based on an approximative self-consistent-field method were used in the present work.

3. Experiment

The single crystals used in this work were supplied by Goodfellow Metals Ltd, England. Both CaO and NaF crystals had the shape of a bar having a length of about 20 mm along the [100] direction and a square cross section of about 150 mm^2. A cut along (100) planes was first made with a diamond wafering saw and then crystals were realigned to cut them along (110) planes. The thickness of each cut was 2·0 mm. The orientation was checked using X-ray diffraction apparatus and it was found to be correct within ±1° in each case.

In order to keep the scattering volume identical to minimize the uncertainties in multiple photon scattering effects, crystals were put behind a lead mask of diameter 10 mm. The spectrometer used in the experiment has been previously described (Manninen & Paakkari, 1978). Briefly, γ-rays from a 5 Ci annular ^{241}Am source are collimated cylindrically and after scattering through a mean angle of 175° by a sample in a vacuum chamber collimated again to be analysed in a system which consists of Ge detector, amplifying electronics and ND-60 multichannel analyser. The channel spacing was set to be about 63 eV (0·1 a.u. of momentum).

A separate measurement using the sample holder and lead mask was first performed to be used for background subtraction. Strictly speaking there is also a contribution to the background which depends on the sample, *i.e.* the continuous *Bremsstrahlung* produced by Compton and photoelectrons. In the present case this turns out to be negligible (see Alexandropoulos, Chatzigeorgiou, Cooper, Evangelakis & Manninen, 1988). Also the pile-up effect due to the higher counting rate in the actual measurement was minimized using pile-up rejection electronics. Each crystal direction was measured three times and altogether about 800 000 counts/channel were gathered at the Compton peak. The stability in the counting chain was checked daily using a small ^{241}Am source in front of the detector. The largest shift allowed in the data was ±0·1 channels.

The data processing consisted of the following steps:

(i) The background spectrum, normalized to the time of the actual measurement, was first subtracted from the measured data.

(ii) A deconvolution procedure was performed to remove the instrumental resolution effects. This was based on the generalized least-squares method described earlier by Paatero, Manninen & Paakkari (1974). The resolution function was measured using a small pinhole-collimated ^{241}Am source. Due to the random noise in the measured data, high frequencies cannot be reproduced in the deconvolution. This leads to a residual instrument function (RIF) and this should be taken into account before any theory is compared with the present experimental data. The RIF of the present experiment is given in Table 2.

(iii) The energy dependence of the absorption in the sample and the differential Compton scattering cross section was calculated according to Manninen, Paakkari & Kajantie (1974).

(iv) A Monte Carlo procedure was applied to remove double-scattering effects from the measured data (Halonen, Williams & Paakkari, 1975). The double/single scattering ratio was about 9·7% for NaF and 11·2% for CaO and the effect of this correction at the peak of the Compton profile 1·5 and 1·7% respectively. In order to minimize the effect of the statistical nature of the Monte Carlo method the following procedure was applied: (*a*) The experimental Compton-profile difference curves were multiplied by the double/single scattering ratio which can be calculated very accurately. Providing that the multiple-scattering contribution is isotropic (which certainly is at least a good approximation), it has the

Table 2. *Residual instrument function (RIF) of the experiment*

p_z (a.u.)	RIF	p_z (a.u.)	RIF
0·0	2·347	1·9	0·023
0·1	2·124	2·0	0·013
0·2	1·537	2·1	0·001
0·3	0·794	2·2	−0·007
0·4	0·133	2·3	−0·010
0·5	−0·277	2·4	−0·006
0·6	−0·392	2·5	−0·001
0·7	−0·287	2·6	0·003
0·8	−0·091	2·7	0·004
0·9	0·074	2·8	0·003
1·0	0·145	2·9	0·001
1·1	0·124	3·0	−0·001
1·2	0·052	3·1	−0·002
1·3	−0·018	3·2	−0·001
1·4	−0·055	3·3	0·000
1·5	−0·053	3·4	0·000
1·6	−0·027	3·5	0·001
1·7	0·002	3·6	0·000
1·8	0·021		

Table 3. *Experimental Compton profiles of* NaF *and* CaO

The statistical error limit is given for some points. The profiles are not corrected for multiple-scattering effects.

p_z	NaF		CaO	
(a.u.)	$J_{100}(\sigma)$	J_{110}	$J_{100}(\sigma)$	J_{110}
0·0	5·400 (0·007)	5·397	7·487 (0·011)	7·429
0·1	5·385	5·372	7·456	7·398
0·2	5·328	5·312	7·362	7·305
0·3	5·227	5·217	7·200	7·148
0·4	5·084	5·086	6·967	6·932
0·5	4·902	4·920	6·660	6·667
0·6	4·689	4·719	6·288	6·358
0·7	4·454	4·486	5·873	6·001
0·8	4·201	4·225	5·441	5·596
0·9	3·938	3·944	5·017	5·149
1·0	3·668 (0·006)	3·652	4·612 (0·008)	4·679
1·1	3·395	3·359	4·225	4·206
1·2	3·124	3·076	3·853	3·755
1·3	2·861	2·812	3·492	3·354
1·4	2·611	2·573	3·140	3·015
1·5	2·376	2·360	2·805	2·733
1·6	2·160	2·172	2·500	2·494
1·7	1·965	2·003	2·238	2·287
1·8	1·793	1·846	2·025	2·103
1·9	1·643	1·699	1·861	1·940
2·0	1·514 (0·004)	1·561	1·738 (0·006)	1·800
2·2	1·306	1·314	1·559	1·573
2·4	1·140	1·123	1·410	1·379
2·6	0·995	0·977	1·268	1·229
2·8	0·866	0·856	1·141	1·131
3·0	0·751 (0·003)	0·748	1·036 (0·004)	1·045
3·5	0·557	0·560	0·854	0·849
4·0	0·433	0·428	0·723	0·721
4·5	0·346	0·347	0·617	0·615
5·0	0·281 (0·002)	0·278	0·519 (0·003)	0·516
6·0	0·197	0·196	0·375	0·373
7·0	0·137 (0·001)	0·137	0·278 (0·002)	0·276

Table 4. *Theoretical Compton profiles of* NaF *and* CaO

The profiles J_1 and J_2 correspond to the APW calculation with and without the Lam–Platzman correction, respectively. J_3 denotes the corresponding LCAO profile [Na^+, Ca^{2+} and F^- wave functions of Clementi (1965) and O^{2-} wave function of Pantelides *et al.* (1974)]. Columns J_4–J_6 refer to the corresponding conditions for the [110] direction.

(*a*) NaF

p_z	100			110		
(a.u.)	J_1	J_2	J_3	J_4	J_5	J_6
0·0	5·595	5·662	5·555	5·598	5·659	5·568
0·1	5·576	5·646	5·535	5·581	5·650	5·550
0·2	5·520	5·591	5·476	5·529	5·603	5·495
0·3	5·423	5·490	5·375	5·440	5·513	5·400
0·4	5·281	5·338	5·232	5·309	5·366	5·264
0·5	5·097	5·137	5·049	5·133	5·165	5·085
0·6	4·871	4·893	4·830	4·911	4·924	4·865
0·7	4·612	4·619	4·582	4·649	4·651	4·609
0·8	4·329	4·324	4·314	4·351	4·354	4·324
0·9	4·035	4·023	4·036	4·031	4·036	4·020
1·0	3·735	3·725	3·752	3·699	3·702	3·709
1·1	3·439	3·435	3·469	3·372	3·368	3·401
1·2	3·148	3·152	3·190	3·060	3·049	3·106
1·3	2·867	2·872	2·916	2·775	2·763	2·831
1·4	2·598	2·598	2·651	2·521	2·513	2·581
1·5	2·344	2·335	2·400	2·299	2·293	2·358
1·6	2·111	2·095	2·166	2·105	2·099	2·160
1·7	1·903	1·887	1·955	1·936	1·928	1·983
1·8	1·721	1·710	1·769	1·783	1·776	1·822
1·9	1·568	1·560	1·608	1·643	1·635	1·674
2·0	1·438	1·434	1·472	1·511	1·503	1·536
2·2	1·239	1·231	1·256	1·273	1·261	1·288
2·4	1·088	1·075	1·091	1·076	1·065	1·084
2·6	0·959	0·949	0·952	0·925	0·916	0·927
2·8	0·840	0·833	0·830	0·811	0·801	0·807
3·0	0·727	0·717	0·718	0·716	0·707	0·709
3·5	0·512	0·505	0·507	0·524	0·516	0·514
4·0	0·405	0·398	0·396	0·406	0·400	0·397
4·5	0·324	0·319	0·318	0·318	0·313	0·313
5·0	0·254	0·251	0·250	0·257	0·254	0·253
6·0	0·174	0·172	0·174	0·174	0·172	0·172
7·0	0·120	0·120	0·120	0·120	0·120	0·120

(*b*) CaO

p_z	100			110		
(a.u.)	J_1	J_2	J_3	J_4	J_5	J_6
0·0	7·744	7·795	8·064	7·662	7·727	8·041
0·1	7·721	7·782	8·033	7·638	7·723	8·014
0·2	7·644	7·725	7·933	7·563	7·666	7·929
0·3	7·496	7·600	7·758	7·432	7·540	7·779
0·4	7·261	7·383	7·498	7·237	7·323	7·554
0·5	6·934	7·056	7·155	6·971	7·023	7·248
0·6	6·525	6·608	6·741	6·632	6·656	6·862
0·7	6·064	6·068	6·277	6·223	6·238	6·404
0·8	5·584	5·515	5·790	5·754	5·772	5·889
0·9	5·115	5·030	5·302	5·245	5·263	5·339
1·0	4·672	4·628	4·826	4·719	4·715	4·779
1·1	4·256	4·277	4·367	4·204	4·173	4·234
1·2	3·858	3·929	3·922	3·723	3·691	3·728
1·3	3·471	3·529	3·492	3·296	3·273	3·278
1·4	3·092	3·076	3·080	2·932	2·919	2·893
1·5	2·733	2·656	2·696	2·631	2·622	2·574
1·6	2·409	2·335	2·354	2·386	2·376	2·314
1·7	2·136	2·100	2·067	2·186	2·171	2·103
1·8	1·920	1·920	1·838	2·016	2·000	1·928
1·9	1·760	1·772	1·666	1·869	1·853	1·778
2·0	1·643	1·648	1·540	1·735	1·720	1·646
2·2	1·484	1·458	1·375	1·506	1·485	1·428
2·4	1·355	1·326	1·261	1·326	1·308	1·266
2·6	1·230	1·221	1·167	1·196	1·179	1·155
2·8	1·114	1·102	1·085	1·097	1·082	1·071
3·0	1·010	0·992	1·008	1·011	0·998	0·994
3·5	0·830	0·825	0·822	0·831	0·824	0·819
4·0	0·701	0·697	0·681	0·702	0·698	0·692
4·5	0·590	0·587	0·579	0·590	0·588	0·575
5·0	0·500	0·499	0·484	0·499	0·497	0·482
6·0	0·354	0·353	0·336	0·355	0·353	0·335
7·0	0·255	0·253	0·235	0·255	0·253	0·237

same effect on all directional profiles and can therefore be treated as a multiplicative factor in the normalization of each profile. (*b*) The B functions were calculated from the experimental data before multiple scattering correction. Owing to the broad momentum distribution of the multiple scattering profile this does not introduce any noticeable error in the valence-electron region of the position space. (*c*) Directional Compton profiles, corrected for multiple scattering, were also calculated. These include, however, larger statistical error due to point-by-point correction in the Monte Carlo procedure. Also possible systematic errors which largely cancel out after taking a difference are present in individual profiles.

(v) Finally the corrected profiles were normalized to have an area of the theoretical profiles in the momentum range of from −7·0 to +7·0 a.u.

The final experimental profiles, calculated as an average of three measurements, are given in Table 3.

4. Results and discussion

The theoretical Compton profiles for NaF and CaO, as calculated by the APW and the LCAO methods, are given in Tables 4(*a*) and (*b*). To enable comparison with the experimental results these calculated values have been convoluted with the experimental RIF as revealed by Table 2 before any comparison with the experiment. As in most cases at small p_z the theoretical profiles of both methods are too large. The APW profiles J_1 and J_4 of Tables 4(*a*), (*b*) already contain the momentum-space correlation corrections which are isotropic for the local-density-approximation (Lam & Platzman, 1974; Tong & Lam, 1978; Bauer, 1983; Bauer & Schneider, 1983). Therefore they cancel in all differences of profiles and $B(z)$ functions. These corrections were calculated using the occupation numbers for the interacting homogeneous electron gas as listed by Tong & Lam (1978) and the muffin-tin electron density of our APW calculation. Although the correlation corrections go in the right direction they seem to be insufficient. However one should be cautious in comparing the theoretical profiles with the experimental data in Table 3 which are not corrected for multiple-scattering processes. Inclusion of the experimental multiple-scattering corrections would move the experimental data close to the theoretical profiles, very similar to the theoretical correlation corrections. However it should be emphasized that the present experiment was designed to yield accurate results for difference profiles and not for the total quantities.

Earlier isotropic Compton profiles for much thinner NaF samples (Paakkari & Halonen, 1978) clearly support our statement above because the deviation from our averaged directional profiles is reduced by a factor of two. In the case of NaF the APW and LCAO theoretical profiles agree very well whereas for CaO larger discrepancies can be observed because the LCAO profiles are narrower. They are larger by 4% at $p_z = 0$ and smaller by 6% at $p_z = 2$. Furthermore, the differences of APW and LCAO total profiles are direction dependent because for the [110] direction the APW minus LCAO curve is smooth but shows oscillatory components for the [100] profile. Interestingly, for both NaF and CaO the wave functions used for the Compton profiles were derived from local-orbital Hartree-Fock-type band-structure calculations.

After convoluting and taking the difference $J_{100}(p_z) - J_{110}(p_z)$, one is left with the anisotropy curve which is shown in Fig. 1 for NaF and in Fig. 2 for CaO. As can be seen in Fig. 1, both theories give almost identical results but neither agree very well with the experimental anisotropy showing the largest deviations at small p_z and also for the largest peak at 1·2 a.u. Similar deviations were found for MgO (Aikala *et al.*, 1982; Podloucky & Redinger, 1984). This is surprising for NaF, because it is supposed to be an almost ideal candidate for an ionic crystal and because in the case of the spherically averaged Compton profiles the agreement between the experiment and LCAO model was good (Paakkari & Halonen, 1978). Because the LCAO profiles for NaF compare very well with the APW results one might conclude that if the LCAO model contains a suitable ionic configuration and a correct orthogonalization procedure then a good answer is obtained.

In the case of CaO, Fig. 2 shows the APW results and the experiment in excellent agreement, whereas the LCAO model does not seem to work very well especially at small p_z. One reason for that might be the choice of the O^{2-} ionic wave function employed in the LCAO model which was taken from MgO calculations. The lattice-parameter difference is quite large (7·9596 a.u. for MgO, 9·0907 a.u. for CaO) and this certainly has some effect on the quality of LCAO results for CaO.

Comparison in position space, *i.e.* in terms of the autocorrelation function, is shown in Fig. 3 for NaF and in Fig. 4 for CaO for the [100] direction. For filled-band systems (Schülke, 1977) as in our case $B(z)$ should be zero at values of z corresponding to a non-zero lattice vector. This property of $B(z)$ can be used to check the quality of a particular experiment or theoretical model. The necessary zero passages of $B(z)$ at L_{100} (Figs. 3 and 4) are correctly reproduced by the experimental data although one should note

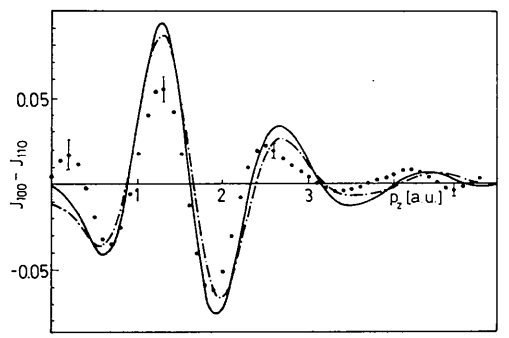

Fig. 1. Difference between the directional Compton profiles $J_{100} - J_{110}$ of NaF. The experimental result is given by dots and the statistical error bars are shown at some points. The solid line corresponds to the APW model and the dash-dotted line to the LCAO calculation. Both theoretical results are convoluted with the residual instrument function of the experiment.

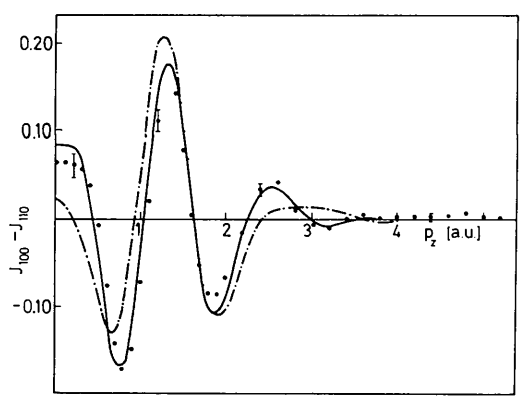

Fig. 2. Difference between the directional Compton profiles $J_{100} - J_{110}$ of CaO. For further explanation, see caption for Fig. 1.

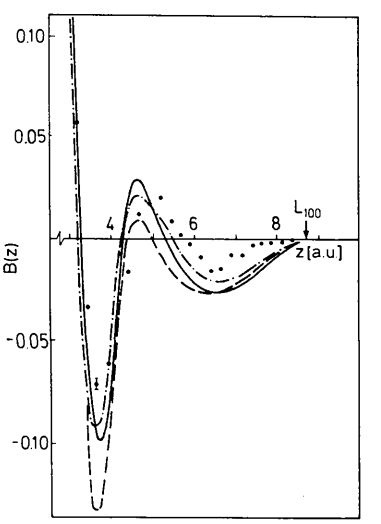

Fig. 3. Fourier transform of the Compton profile of NaF along the [100] direction. L_{100} denotes the 100 lattice site. The solid line shows the results of the APW model before and the dashed line after the Lam-Platzman correction. The LCAO results are given by the dash-dotted curve.

that because of the experimental resolution the accuracy is limited at these distances. Both theoretical $B(z)$ curves show the required zeros at L_{100} agreeing reasonably well in the case of NaF (Fig. 3) but showing significant differences for CaO (Fig. 4). Below $z = 5$ a.u. the APW results have smaller amplitudes than the LCAO results, agreeing better with experiment. The situation is reversed for $z > 5{\cdot}5$ a.u.

The effect of different wave functions of O^{2-}, mentioned in § 2.2, was checked in the LCAO calculations. It turned out that for all cases the overall momentum anisotropy, similar to the experimental one, was obtained. This is apparently due to the correct inclusion of the crystal structure. The differences in terms of the Compton profile anisotropy occurred in the momentum range of 0–2 a.u. and the best agreement with the experiment was obtained using wave functions of Pantelides, Mickish & Kunz (1974). The differences were not large, being everywhere in the band $\Delta J \leq 0{\cdot}02$ in the scale of Fig. 2. In terms of the B functions the comparison remained very similar, except that the Watson model gave the best agreement with the experiment. The situation is then analogous to the MgO results. One should remember, however, that the differences resulting from the use of various O^{2-} wave functions are much smaller than the general discrepancy between the LCAO model and experiment in CaO.

In Figs. 5 and 6 we show the $B(z)$ differences [110]−[100] for both NaF and CaO. Because the theoretical $B(z)$ difference [110]−[111] is of the order of the experimental error (see Tables 4*a* and *b*) the only significant differences are those including the [100] $B(z)$ functions similar to MgO (Aikala, Paakkari & Manninen, 1982; Podloucky & Redinger, 1984). In view of the Compton-profile differences shown in Figs. 1 and 2 it is not surprising that the agreement between the APW model and the experiment is excellent for CaO but less satisfactory for NaF. Regarding the agreement between the two theoretical models there is close agreement for NaF and a rather large difference in the case of CaO. It is interesting to note that for CaO the difference between APW and LCAO is biggest for z between 1 and 4 a.u., whereas in the case of NaF both models agree with each other but disagree with the experimental data.

Returning to the [100] $B(z)$ functions (Figs. 3 and 4) we observe big negative dips before $z = 4$ a.u. due to the overlap of the anion p-like wave functions with their orthogonalization tails around the cations as studied in detail for MgO (Causa, Dovesi, Pisani & Roetti, 1986). Also $B(z)$ is zero close to the nearest-neighbour distance (half of the lattice spacing), reflecting again the orthogonality constraints for the anion p-like wave function with respect to the cation core. The second negative dip at about $z = 7$ a.u. corresponds to the autocorrelation of the anion $p\sigma$-like wave functions. This dip is much more pronounced

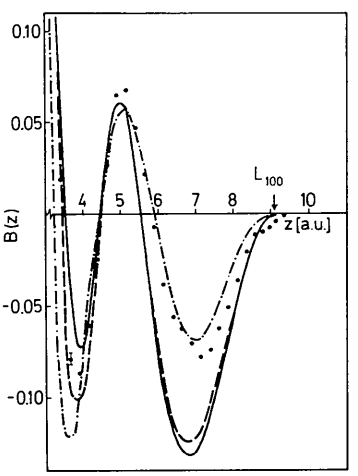

Fig. 4. Fourier transform of the Compton profile of CaO along [100]. For further explanation, see caption for Fig. 3.

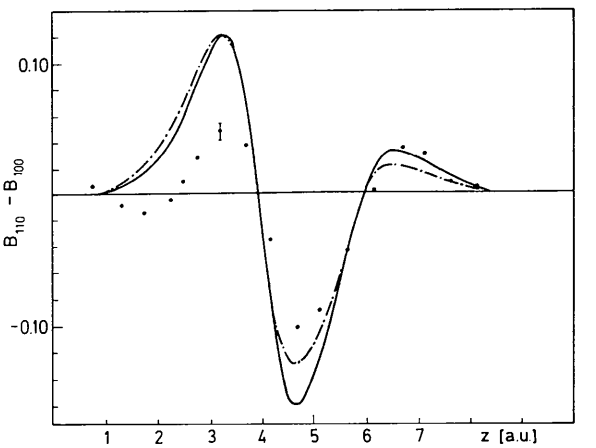

Fig. 5. Difference between the Fourier transformed Compton profiles $B_{110} - B_{100}$ of NaF. For further explanation, see caption for Fig. 1.

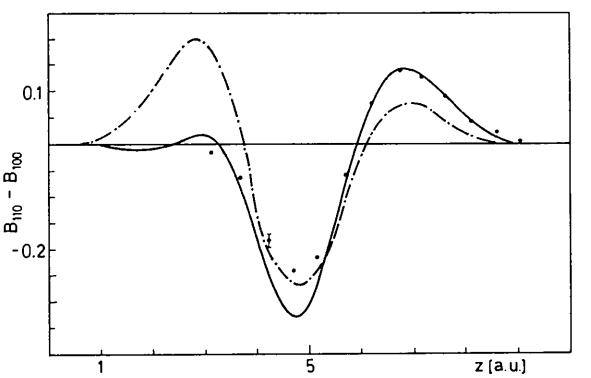

Fig. 6. Difference between the Fourier transformed Compton profiles $B_{110} - B_{100}$ of CaO. For further explanation, see caption for Fig. 1.

Table 5. *Partial charges in the* O (F) 2*p-valence band*

	CaO	NaF	MgO
q_A^p (p-like charge inside the anion sphere)	4·74	5·47	4·91
q_C^s (s-like charge inside the cation sphere)	0·05	0·03	0·06
q_C^p (p-like charge inside the cation sphere)	0·13	0·05	0·08
q_C^d (d-like charge inside the cation sphere)	0·22	0·02	0·03

for CaO than for NaF because the O^{2-} wave function is more spread out than the more compact F^- function. For NaF (Fig. 3) both theoretical curves agree well with experiment whereas for CaO (Fig. 4) remarkable deviations of theoretical curves and experiment as well as differences between the theoretical results are found. The too-large amplitude of the second dip around $z = 7$ a.u. for the APW model indicates that the O atom p wave function is not sufficiently localized. However, the first dip around $z = 4$ a.u. connected to the anion-cation orthogonalization effects is much better described by the APW model. The LCAO model seems to overestimate these orthogonalization effects because the Ca core should be too repulsive due to the missing $3d$ character which is automatically taken care of by the APW *Ansatz* for the crystal wave function. That this $3d$ influence is not negligible is shown by Table 5 which lists partial l-like charges within the APW muffin-tin spheres. With respect to the second dip the smaller amplitude of the LCAO $B(z)$ function compared with the APW results may be explained by the use of the more contracted O^{2-} wave function (corresponding to MgO with a smaller lattice spacing).

From the directional differences of $B(z)$ (Fig. 6) and the previous discussion for CaO we learn that the APW model makes a rather isotropic error by yielding a too diffuse O^{2-} p-like wave function. This error cancels to a large extent resulting in a good agreement with experiment for differences of $B(z)$ functions. In contrast the LCAO model seems to build up more anisotropic errors.

In the case of differences of $B(z)$ functions for NaF (Fig. 5) both theories are in good agreement with each other but deviate from experiment especially for z smaller than 4 a.u. This is the region where the total $B(z)_{[100]}$ (Fig. 3) has the largest negative amplitude which is due to the orthogonalization tail of the F^- $2p$ wave function. It is worthwhile to note that this discrepancy between theory and experiment is very similar to the case of MgO (Aikala, Paakkari & Manninen, 1982; Podloucky & Redinger, 1984) but distinctly different from CaO. It is obvious that one should attribute this exceptional behaviour of CaO as compared to NaF and even MgO to the larger and softer cation Ca^{2+} core.

5. Concluding remarks

Directional Compton profiles of CaO and NaF were measured using an intensive γ-ray source. Applying two different theoretical models, the self-consistent all-electron APW band-structure model within the muffin-tin approximation and the LCAO model based on orthogonalized ionic wave functions, we calculated total directional Compton profiles and $B(z)$ functions including the isotropic Lam-Platzman many-body corrections. From this the corresponding directional differences were obtained. In summary, as in many other cases we find that the nearest-neighbour direction is responsible for some remarkable differences between experimental and theoretical results in the momentum space (Compton profiles) as well as in real space [$B(z)$ autocorrelation functions]. In the case of NaF both theories agree rather well with each other but deviate systematically from the experimental data. For CaO the situation is quite different because the theories show distinct deviations between each other while the directional differences of profiles and autocorrelation functions are correctly reproduced by the APW model. The LCAO model seems to have some difficulties treating the wave functions within the Ca core region. Remaining within the local-density approximation one might consider improving the APW model by going beyond the muffin-tin approximation. The LCAO model should perhaps be extended to a self-consistent treatment allowing for a response of the system to the orthogonalization of the ionic wave functions.

JR and RP would like to acknowledge a grant by the Austrian Ministry of Science (G.Z. 49. 554/3-24/87).

References

ABARENKOV, I. V. & ANTONOVA, I. M. (1979). *Phys. Status Solidi B*, **93**, 315-323.
AIKALA, O. (1977). Report D1. Department of Physical Science, Univ. of Turku, Turku, Finland.
AIKALA, O. (1983). *J. Phys. C*, **16**, 2217-2223.
AIKALA, O., PAAKKARI, T. & MANNINEN, S. (1982). *Acta Cryst.* A**38**, 155-161.
ALEXANDROPOULOS, N. G., CHATZIGEORGIOU, T., COOPER, M. J., EVANGELAKIS, G. & MANNINEN, S. (1988). *Nucl. Instrum. Methods*, A**271**, 543-545.
BAUER, G. E. W. (1983). *Phys. Rev. B*, **27**, 5912-5918.
BAUER, G. E. W. & SCHNEIDER, J. R. (1983). *Solid State Commun.* **47**, 673-676.
CAUSA, M., DOVESI, R., PISANI, C. & ROETTI, C. (1986). *Phys. Rev. B*, **34**, 2939-2941.
CLEMENTI, E. (1965). *Tables of Atomic Functions*. Suppl. to *IBM J. Res. Dev.* **9**, 2-19.
HALONEN, V., WILLIAMS, B. G. & PAAKKARI, T. (1975). *Phys. Fenn.* **10**, 107-122.
LAM, L. & PLATZMAN, P. M. (1974). *Phys. Rev. B*, **9**, 5122-5132.
LÖWDIN, P. O. (1956). *Adv. Phys.* **5**, 1-172.
MANNINEN, S. & PAAKKARI, T. (1978). *Nucl. Instrum. Methods*, **155**, 115-119.
MANNINEN, S., PAAKKARI, T. & KAJANTIE, K. (1974). *Philos. Mag.* **29**, 167-178.
PAAKKARI, T. & HALONEN, V. (1978). *Phys. Scr.* **17**, 433-437.
PAATERO, P., MANNINEN, S. & PAAKKARI, T. (1974). *Philos. Mag.* **30**, 1281-1294.

PANTELIDES, S. T., MICKISH, D. J. & KUNZ, A. B. (1974). *Phys. Rev. B*, **10**, 5203-5212.
PATTISON, P. & WEYRICH, W. (1979). *J. Phys. Chem. Solids*, **40**, 213-222.
PODLOUCKY, R. & REDINGER, J. (1984). *J. Phys. C*, **16**, 6955-6969.
REDINGER, J. & SCHWARZ, K. (1981). *Z. Phys. B*, **40**, 269-276.
SCHÜLKE, W. (1977). *Phys. Status Solidi B*, **82**, 229-235.
SCHWARZ, K. & SCHULZ, H. (1978). *Acta Cryst.* A**34**, 994-999.
TONG, B. Y. & LAM, L. (1978). *Phys. Rev. A*, **18**, 552-558.
WATSON, R. E. (1958). *Phys. Rev.* **111**, 1108-1110.
WILLIAMS, B. G. (1977). Editor. *Compton Scattering*. London: McGraw-Hill.

Acta Cryst. (1989). A**45**, 485-490

New Surface Patches for Minimal Balance Surfaces. III. Infinite Strips

BY WERNER FISCHER AND ELKE KOCH

Institut für Mineralogie der Universität Marburg, Hans-Meerwein-Strasse, D-3550 Marburg, Federal Republic of Germany

(*Received* 1 *December* 1988; *accepted* 7 *March* 1989)

Abstract

Two new families of minimal balance surfaces are described. Their surface patches are not finite but have the shape of infinite strips. Such a strip is bounded by two congruent zigzag lines in one case or by a zigzag line and a meander line in the other case. In addition, certain minimal balance surfaces derived before with the aid of finite surface patches can also be generated from infinite strip-like surface patches.

1. Introduction

A minimal balance surface subdivides R^3 into two disjunct congruent and multiply connected labyrinths (Fischer & Koch, 1987). With one exception, the Y^* or gyroid surface (*cf.* Schoen, 1970; Fischer & Koch, 1987), all minimal balance surfaces known to the authors contain a so-called linear skeletal net, *i.e.* a set of twofold axes totally embedded within the surface.

On the other hand, an appropriate set of twofold axes, *i.e.* a set of twofold axes defined by a group-subgroup pair of space groups with index 2, may be used as generating linear net for one or several minimal balance surfaces. All conceivable sets of such twofold axes have been tabulated before (Koch & Fischer, 1988).

If all twofold axes within such a set are three-dimensionally connected, in general skew circuits may be found that may be spanned disc-like by a patch of a minimal surface. The families of such minimal balance surfaces have been derived completely (Fischer & Koch, 1987; Koch & Fischer, 1988).

So far, three kinds of surface patches have been described for sets of twofold axes disintegrating into parallel flat nets: catenoids (Koch & Fischer, 1988), branched catenoids (Fischer & Koch, 1989), and multiple catenoids (Koch & Fischer, 1989). Each such surface patch is spanned by two flat polygons as generating circuits. These polygons may be either convex or concave with one point of self-contact.

In addition, a fourth kind of surface patch is compatible with parallel flat nets of twofold axes, namely strips of infinite length. Instead of two polygons such a strip is bounded by two infinite zigzag or meander lines which play a role analogous to that of the generating circuits of finite surface patches.

2. Strip-like surface patches

Strip-like surface patches are compatible exclusively with those sets of twofold axes which consist of parallel square or rectangular nets [cases 24, 26, 27, 29, 30 and 32 in Table 1 of Koch & Fischer (1988)]. As one direction parallel to the nets is necessarily distinguished as the infinite direction of the strips, only twofold rotation axes perpendicular to the nets are compatible with strip-like surface patches. Three-, four- and sixfold rotation axes would necessarily give rise to intersection of the strips and, therefore, to self-intersection of the generated minimal surface.

Each strip is bounded by a first zigzag or meander line formed within one quadrangular net and a second such line from a neighbouring net. With respect to the underlying quadrangular nets zigzag lines run in diagonal directions whereas meander lines extend parallel to the twofold axes forming the nets. The two boundary lines of a strip-like surface patch must run parallel and their middle lines must be located directly above each other.

In this way strips of seven different kinds may be constructed. For five kinds the shape of the strips is such that additional twofold axes occur which are embedded within the strips. As a consequence, the linear skeletal net of a minimal balance surface built

0108-7673/89/070485-06$03.00